AAS 20-719

ORBITAL RENDEZVOUS AND SPACECRAFT LOITERING IN THE EARTH-MOON SYSTEM

Fouad Khoury* **and Kathleen C. Howell†**

To meet the challenges posed by future space exploration activities, relative satellite motion techniques and capabilities require development to incorporate dynamically complex regimes. In this investigation, relative motion in the restricted 3-body problem is formulated, validated, and tested to produce solutions to rendezvous and space loitering problems in the Earth-Moon system. Numerical techniques including targeting algorithms are explored to generate relative trajectories between two spacecraft in a 9:2 L_2 Near Rectilinear Halo Orbit (NRHO) as well as spacecraft in a large Distant Retrograde Orbit (DRO).

INTRODUCTION

Relative satellite motion plays a key role in both manned and unmanned space missions. It encompasses a wide array of on-orbit capabilities including rendezvous, proximity operations, docking, and formation flying. Rendezvous operations are typically accomplished by maneuvering a chaser spacecraft to intercept a target. In formation flying, a deputy spacecraft usually operates in the vicinity of a chief vehicle. Relative motion in the two-body problem has been investigated and validated extensively, for a wide variety of missions largely for applications in Low Earth Orbit (LEO) and Geostationary Orbit (GEO). A useful example that represents these 2-body models is rendezvous and docking with the International Space Station (ISS) involving both crewed and uncrewed supply missions. Among the dynamical models that are the most widely applied are the Euler Hill [2] equations (also denoted as the Hill-Clohessy-Wiltshire (HCW) equations) introduced in 1960 for the design of a terminal rendezvous guidance strategy for circular orbits. More recent extensions include the Yamanaka-Ankerson STM [3] approximations for arbitrary elliptical orbits. Although these models demonstrate continued success in space missions appropriate to their respective regimes, they generate unacceptable errors in their descriptions of relative orbits that exist with the incorporation of both Earth and Moon gravity fields as point masses. Incorporation of both the Earth and Moon gravity is necessary in formulations for relative motion analysis for orbits in models with increased dynamical complexity.

Franzini et al. [1] initially formulated the nonlinear equations of relative motion for the restricted 3-body problem in the local vertical local horizontal (LVLH) frame attached to the target spacecraft. In this investigation, the equations of relative motion are applied to a target trajectory along a L_2 NRHO and a large DRO. A number of rendezvous scenarios are investigated for close proximity configurations between the target and chaser spacecraft. These equations are validated for the 9:2

*M.S. Student, School of Aeronautics and Astronautics, Purdue University, West Lafayette, IN 47907 email: fkhoury@purdue.edu

†Hsu Lo Distinguished Professor of Aeronautics and Astronautics, School of Aeronautics and Astronautics, Purdue University, West Lafayette, IN 47907 email: howell@purdue.edu

L_2 NRHO and a large DRO, orbits that may both be options for NASA's Gateway and Artemis programs, with the aim of establishing an orbiting lunar platform in the vicinity of the Moon. Moreover, a framework is developed to incorporate targeting strategies to yield the desired relative geometry for a variety of rendezvous scenarios. Analysis and recommendations for spacecraft loitering near the target are also examined for the various orbit geometries. Solutions are computed in both the Circular Restricted 3-Body Problem (CR3BP) and Elliptical Restricted 3-Body Problem (ER3BP) as the dynamical models for the Earth-Moon dynamics.

EARTH-MOON DYNAMICS

In this investigation, the restricted three-body problem is employed to model the Earth-Moon system. The model is comprised of two primaries, with masses m_1 and m_2, and a body of interest with mass m. Traditionally, the equations of motion for the restricted three-body problem are written in a synodic frame S attached to the system barycenter. Figure 1 depicts the general three-body problem with inertial frame I and synodic frame S. Note that each frame is defined by unit vectors that are dextral orthonormal triads. The synodic frame S is represented in terms of the axes $\hat{\mathbf{x}}_s, \hat{\mathbf{y}}_s$ and $\hat{\mathbf{z}}_s$. The restricted three-body problem operates on a set of assumptions where all bodies are modeled as point masses and the mass of body m is negligible compared to the masses of the two primaries, m_1 and m_2. As a result, the motion of the primaries are modeled as Keplerian. Note that $\hat{\mathbf{x}}_s - \hat{\mathbf{y}}_s$ is the plane of primary motion.

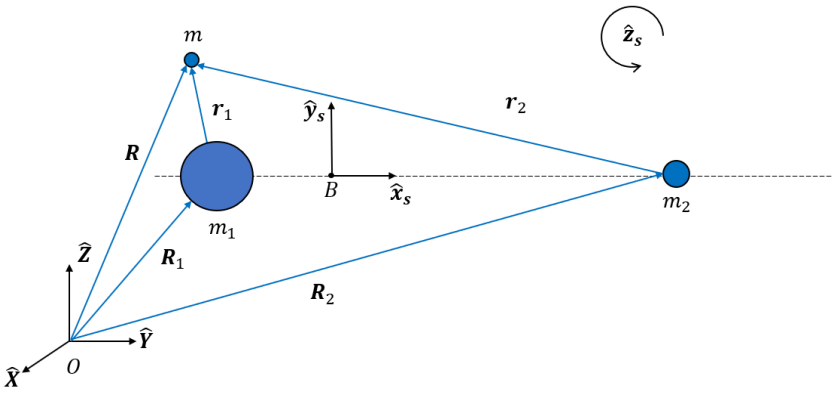

Figure 1. Diagram of the three-body model in synodic frame S.

Newton's law of gravitation is employed to formulate the equations of motion for mass m under the gravitational influence of the two primaries. Consequently, the accelerations of each of the bodies in the problem are written as

$$\underset{I}{[\ddot{\mathbf{R}}]} = -\frac{Gm_1}{r_1^3}\mathbf{r}_1 - \frac{Gm_2}{r_2^3}\mathbf{r}_2 \tag{1}$$

$$\underset{I}{[\ddot{\mathbf{R}}_1]} = \frac{Gm_2}{r_{12}^3}\mathbf{r}_{12} + \frac{Gm}{r_1^3}\mathbf{r}_1 \tag{2}$$

$$\underset{I}{[\ddot{\mathbf{R}}_2]} = -\frac{Gm_1}{r_{12}^3}\mathbf{r}_{12} + \frac{Gm}{r_2^3}\mathbf{r}_2 \tag{3}$$

where $\mathbf{r}_1 = \mathbf{R} - \mathbf{R}_1$ is the relative position vector from m_1 to m, $\mathbf{r}_2 = \mathbf{R} - \mathbf{R}_2$ is the relative position vector from m_2 to m, and $\mathbf{r}_{12} = \mathbf{R}_2 - \mathbf{R}_1$ is the relative position vector from m_1 to m_2. The notation $\underset{I}{\left[\ddot{\mathbf{R}}\right]}$ specifies the acceleration of body m as observed from an inertial frame of reference I. Solving for the accelerations of the relative position vectors yields

$$\underset{I}{\left[\ddot{\mathbf{r}}_1\right]} = -\mu_1 \frac{\mathbf{r}_1}{r_1^3} - \mu_2 \left(\frac{\mathbf{r}_2}{r_2^3} + \frac{\mathbf{r}_{12}}{r_{12}^3} \right) \tag{4}$$

$$\underset{I}{\left[\ddot{\mathbf{r}}_2\right]} = -\mu_2 \frac{\mathbf{r}_2}{r_2^3} - \mu_1 \left(\frac{\mathbf{r}_1}{r_1^3} - \frac{\mathbf{r}_{12}}{r_{12}^3} \right) \tag{5}$$

where $\mu_1 = Gm_1$ and $\mu_2 = Gm_2$ are the gravitational parameters of m_1 and m_2, respectively. Since the mass m is negligible, the two primaries move on conics about their common barycenter. The synodic frame S is assumed to rotate with respect to the inertial frame I with angular velocity $\boldsymbol{\omega}_{S/I} = \omega_{S/I}\hat{\mathbf{z}}_s$. As a result, the basic kinematical equation is employed to compute the velocity and accelerations for vector $\mathbf{R}$, as measured from the system barycenter B, with respect to an inertial observer is expressed as

$$\mathbf{R} = x\hat{\mathbf{x}}_s + y\hat{\mathbf{y}}_s + z\hat{\mathbf{z}}_s \tag{6}$$

$$\underset{I}{\left[\dot{\mathbf{R}}\right]} = \underset{S}{\left[\dot{\mathbf{R}}\right]} + \boldsymbol{\omega}_{S/I} \times \mathbf{R} \tag{7}$$

$$\underset{I}{\left[\ddot{\mathbf{R}}\right]} = \underset{S}{\left[\ddot{\mathbf{R}}\right]} + 2\boldsymbol{\omega}_{S/I} \times \underset{S}{\left[\dot{\mathbf{R}}\right]} + \underset{S}{\left[\dot{\boldsymbol{\omega}}_{S/I}\right]} \times \mathbf{R} + \boldsymbol{\omega}_{S/I} \times (\boldsymbol{\omega}_{S/I} \times \mathbf{R}) \tag{8}$$

Without loss of generality, frames S and I coincide with origins at B so that Equation (1) is substituted into Equation (8) to obtain

$$\underset{S}{\left[\ddot{\mathbf{R}}\right]} + 2\boldsymbol{\omega}_{S/I} \times \underset{S}{\left[\dot{\mathbf{R}}\right]} + \underset{S}{\left[\dot{\boldsymbol{\omega}}_{S/I}\right]} \times \mathbf{R} + \boldsymbol{\omega}_{S/I} \times (\boldsymbol{\omega}_{S/I} \times \mathbf{R}) = -\mu_1 \frac{\mathbf{r}_1}{r_1^3} - \mu_2 \frac{\mathbf{r}_2}{r_2^3} \tag{9}$$

where position vectors $\mathbf{r}_1$ and $\mathbf{r}_2$, measured from the barycenter B, denote the spacecraft position vectors with respect to m_1 and m_2, respectively, as

$$\mathbf{r}_1 = (x + R_1)\hat{\mathbf{x}}_s + y\hat{\mathbf{y}}_s + z\hat{\mathbf{z}}_s \qquad \mathbf{r}_2 = (x - R_2)\hat{\mathbf{x}}_s + y\hat{\mathbf{y}}_s + z\hat{\mathbf{z}}_s$$

In component-wise form along each of the axis directions in frame S, the equations are expressed

$$\ddot{x} - 2\omega_{S/I}\dot{y} - \dot{\omega}_{S/I}y - \omega_{S/I}^2 x = -\mu_1 \frac{x + R_1}{r_1^3} - \mu_2 \frac{x - R_2}{r_2^3} \tag{10}$$

$$\ddot{y} + 2\omega_{S/I}\dot{x} + \dot{\omega}_{S/I}x - \omega_{S/I}^2 y = -\mu_1 \frac{y}{r_1^3} - \mu_2 \frac{y}{r_2^3} \tag{11}$$

$$\ddot{z} = -\mu_1 \frac{z}{r_1^3} - \mu_2 \frac{z}{r_2^3} \tag{12}$$

where the norm of the spacecraft distance from each of the primaries are expressed

$$r_1 = \sqrt{(x+R_1)^2 + y^2 + z^2} \qquad r_2 = \sqrt{(x-R_2)^2 + y^2 + z^2}$$

Equations (10)-(12) represent the elliptical restricted three-body problem (ER3BP) and characterize position vectors with respect to the system barycenter B. For some applications, it is sometimes useful to change the origin of the synodic frame so that the spacecraft position is measured with respect to one of the primaries. Thus, a rotating synodic frame M with axes $\hat{\mathbf{x}}_m, \hat{\mathbf{y}}_m$ and $\hat{\mathbf{z}}_m$ is introduced so that the spacecraft position vector is referenced from the second primary, m_2. Frame M rotates with the same angular velocity as S, yet the axes are defined with different directions such that

$$\hat{\mathbf{x}}_m = -\frac{\mathbf{r}_{12}}{r_{12}} = -\hat{\mathbf{x}}_s \quad \hat{\mathbf{z}}_m = \frac{\mathbf{h}_{12}}{h_{12}} = \hat{\mathbf{z}}_s \quad \hat{\mathbf{y}}_m = \hat{\mathbf{z}}_m \times \hat{\mathbf{x}}_m = -\hat{\mathbf{y}}_s \tag{13}$$

The formulation of synodic frame M is consistent with the definitions in Franzini et al [1]. The positive $\hat{\mathbf{x}}$ direction is directed towards the larger primary m_1 and $\hat{\mathbf{z}}$ is directed such that it is parallel to the orbital angular momentum of the primaries. Figure 2 depicts the differences in synodic frames S and M in the ER3BP. Both frames rotate with the same angular velocity with respect to the inertial frame I, however, they originate at different positions.

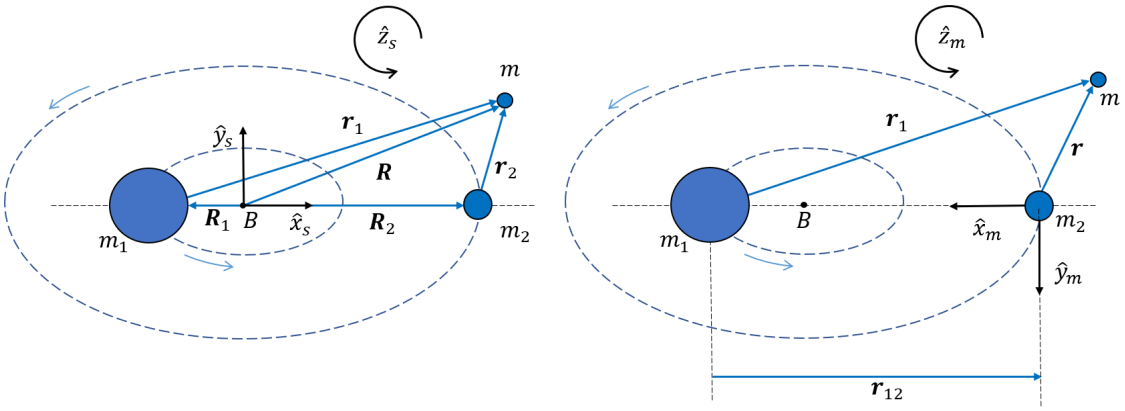

Figure 2. Diagram of the ER3BP in synodic frames S (left) and M (right).

The employment of frame M provides a description of the motion of body m with respect to the second primary m_2. Therefore, without loss of generality, if inertial frame I and synodic frame M coincide at m_2, the position, velocity, and acceleration of spacecraft m as expressed in frame M coordinates are

$$\mathbf{r} = x\hat{\mathbf{x}}_m + y\hat{\mathbf{y}}_m + z\hat{\mathbf{z}}_m \tag{14}$$

$$\underset{I}{[\dot{\mathbf{r}}]} = \underset{M}{[\dot{\mathbf{r}}]} + \boldsymbol{\omega}_{M/I} \times \mathbf{r} \tag{15}$$

$$\underset{I}{[\ddot{\mathbf{r}}]} = \underset{M}{[\ddot{\mathbf{r}}]} + 2\boldsymbol{\omega}_{M/I} \times \underset{M}{[\dot{\mathbf{r}}]} + \underset{M}{[\dot{\boldsymbol{\omega}}_{M/I}]} \times \mathbf{r} + \boldsymbol{\omega}_{M/I} \times (\boldsymbol{\omega}_{M/I} \times \mathbf{r}) \tag{16}$$

where $\mathbf{r}_{12} = -r_{12}\hat{\mathbf{x}}_m$, and the spacecraft position vectors measured from the first and second primaries are defined as

$$\mathbf{r}_1 = (x - r_{12})\hat{\mathbf{x}}_m + y\hat{\mathbf{y}}_m + z\hat{\mathbf{z}}_m \qquad \mathbf{r} = x\hat{\mathbf{x}}_m + y\hat{\mathbf{y}}_m + z\hat{\mathbf{z}}_m$$

In component-wise form, Equation (16) is written as

$$\ddot{x} - 2\omega_{M/I}\dot{y} - \dot{\omega}_{M/I}y - \omega_{M/I}^2 x = -\mu_1\left(\frac{x - r_{12}}{r_1^3} + \frac{1}{r_{12}^3}\right) - \mu_2\frac{x}{r^3} \tag{17}$$

$$\ddot{y} + 2\omega_{M/I}\dot{x} + \dot{\omega}_{M/I}x - \omega_{M/I}^2 y = -\mu_1\frac{y}{r_1^3} - \mu_2\frac{y}{r^3} \tag{18}$$

$$\ddot{z} = -\mu_1\frac{z}{r_1^3} - \mu_2\frac{z}{r^3} \tag{19}$$

where the norm of the distances between the spacecraft and primary m_1 and m_2 are evaluated as

$$r_1 = \sqrt{(x - r_{12})^2 + y^2 + z^2} \qquad r = \sqrt{x^2 + y^2 + z^2}$$

In this investigation, nondimensional quantities are used so that the equations of motion become functions of one parameter. Nondimensionalization for the ER3BP equations of motion is accomplished by normalizing the following:

- dimensional distances l by the primary m_2 orbit semimajor axis a
- time t by the system mean motion n, i.e.,

$$n = \sqrt{\frac{G(m_1 + m_2)}{a^3}} \tag{20}$$

  and the introduction of a nondimensional time quantity τ such that $\tau = n(t - t_0)$
- mass quantities such that $\mu_1 + \mu_2 = 1$

As a consequence, any generic distance and its corresponding time derivatives are nondimensionalized as follows

$$l = a\tilde{l} \qquad \dot{l} = a\frac{d\tilde{l}}{d\tau}\frac{d\tau}{dt} = an\tilde{l}' \qquad \ddot{l} = an\frac{d\tilde{l}'}{d\tau}\frac{d\tau}{dt} = an^2\tilde{l}''$$

where the quantities under the tilde symbol, i.e. $\tilde{l}$, denote nondimensional quantities and the superscript prime symbol, i.e. $\tilde{l}'$, represents derivatives with respect to τ. Angular quantities ω are nondimensionalized using a similar procedure, so it follows that

$$\omega = n\tilde{\omega} \qquad \dot{\omega} = \frac{d\omega}{d\tau}\frac{d\tau}{dt} = n^2\tilde{\omega}'$$

The system mass parameter is defined as $\mu = m_2/(m_1 + m_2)$, therefore, the mass parameters for the primaries m_1 (representing the Earth) and m_2 (representing the Moon) are expressed as

$$\mu_M = \mu \qquad\qquad \mu_E = 1 - \mu \tag{21}$$

The scalar nondimensional equations of motion in the ER3BP then follow, expressed in terms of components in Frame S as,

$$\tilde{x}'' - 2\tilde{\omega}_{S/I}\tilde{y}' - \tilde{\omega}'_{S/I}\tilde{y} - \tilde{\omega}^2_{S/I}\tilde{x} = -(1-\mu)\frac{\tilde{x} + \tilde{R}_1}{\tilde{r}_1^3} - \mu\frac{\tilde{x} - \tilde{R}_2}{\tilde{r}_2^3} \tag{22}$$

$$\tilde{y}'' + 2\tilde{\omega}_{S/I}\tilde{x}' + \tilde{\omega}'_{S/I}\tilde{x} - \tilde{\omega}^2_{S/I}\tilde{y} = -(1-\mu)\frac{\tilde{y}}{\tilde{r}_1^3} - \mu\frac{\tilde{y}}{\tilde{r}_2^3} \tag{23}$$

$$\tilde{z}'' = -(1-\mu)\frac{\tilde{z}}{\tilde{r}_1^3} - \mu\frac{\tilde{z}}{\tilde{r}_2^3} \tag{24}$$

Likewise, the ER3BP equations in terms of Frame M in nondimensional form are defined as

$$\tilde{x}'' - 2\tilde{\omega}_{M/I}\tilde{y}' - \tilde{\omega}'_{M/I}\tilde{y} - \tilde{\omega}^2_{M/I}\tilde{x} = -(1-\mu)\left(\frac{\tilde{x} - \tilde{r}_{12}}{\tilde{r}_1^3} + \frac{1}{\tilde{r}_{12}^2}\right) - \mu\frac{\tilde{x}}{\tilde{r}^3} \tag{25}$$

$$\tilde{y}'' + 2\tilde{\omega}_{M/I}\tilde{x}' + \tilde{\omega}'_{M/I}\tilde{x} - \tilde{\omega}^2_{M/I}\tilde{y} = -(1-\mu)\frac{\tilde{y}}{\tilde{r}_1^3} - \mu\frac{\tilde{y}}{\tilde{r}^3} \tag{26}$$

$$\tilde{z}'' = -(1-\mu)\frac{\tilde{z}}{\tilde{r}_1^3} - \mu\frac{\tilde{z}}{\tilde{r}^3} \tag{27}$$

There are advantages to analysis based in the ER3BP in either frame S and frame M, largely dependent on the type of application. Selected orbits in close proximity to the second primary can employ the M frame since it is expected that the spacecraft position is measured from m_2 and not the barycenter B. Moreover, nondimensional quantities are useful since they alleviate computational expense by parameterizing equations with respect to one value, namely μ. For simplicity, the tilde sign $(\tilde{x})$ is dropped from equations with the understanding that all quantities subsequently discussed in this document are nondimensional.

Circular Restricted Three-Body Problem (CR3BP)

A further assumption in addition to those governing the ER3BP offers an additional reduction of the restricted three-body problem, the CR3BP. The primaries m_1 and m_2 are already assumed to move on a Keplerian orbit. Now, the conic motion of the primaries is further assumed to be circular orbits about their common barycenter. Under this assumption, there are two main simplications:

- The nondimensional angular velocity for both synodic frames S and M are $\omega_{S/I} = \omega_{M/I} = 1$
- The distance between the two primaries is constant, thus

$$\mathbf{R}_1 = -\mu\hat{\mathbf{x}}_s \qquad \mathbf{R}_2 = (1-\mu)\hat{\mathbf{x}}_s \qquad \mathbf{r}_{12} = \hat{\mathbf{x}}_s = -\hat{\mathbf{x}}_m \tag{28}$$

If the assumptions described in the CR3BP are applied, Equations (22) - (24) in the S frame are reduced to

$$x'' - 2y' - x = -(1-\mu)\frac{x+\mu}{r_1^3} - \mu\frac{x-1+\mu}{r_2^3} \tag{29}$$

$$y'' + 2x' - y = -(1-\mu)\frac{y}{r_1^3} - \mu\frac{y}{r_2^3} \tag{30}$$

$$z'' = -(1-\mu)\frac{z}{r_1^3} - \mu\frac{z}{r_2^3} \tag{31}$$

where,

$$r_1 = \sqrt{(x+\mu)^2 + y^2 + z^2} \qquad r_2 = \sqrt{(x-1+\mu)^2 + y^2 + z^2}$$

Likewise, Equations (25) - (27) in the M frame then become

$$x'' - 2y' - x = -(1-\mu)\left(\frac{x-1}{r_1^3} + 1\right) - \mu\frac{x}{r^3} \tag{32}$$

$$y'' + 2x' - y = -(1-\mu)\frac{y}{r_1^3} - \mu\frac{y}{r^3} \tag{33}$$

$$z'' = -(1-\mu)\frac{z}{r_1^3} - \mu\frac{z}{r^3} \tag{34}$$

where,

$$r_1 = \sqrt{(x-1)^2 + y^2 + z^2} \qquad r = \sqrt{x^2 + y^2 + z^2}$$

The CR3BP assumes that both the distances between the primaries and the nondimensional angular velocity of frames S and M remain constant, greatly simplifying the equations of motion.

REFERENCE ORBITS

Two specific reference orbits that exist in the CR3BP are considered for relative motion analysis in this investigation. The first reference orbit is the 9:2 L_2 NRHO with a period of 6.5 days, a perilune of about 3,250 km, and an apolune of approximately 71,000 km. The 9:2 L_2 NRHO is currently selected as the baseline orbit for the Gateway platform due to its favorable stability properties and eclipse avoidance properties. The second reference orbit is a large DRO with a period of 14.2 days, a average perilune distance of 71,700 km, and an average apolune distance of approximately

98,500 km. The large DRO is a proposed reference orbit for the Artemis I mission along which the Orion spacecraft is expected to implement orbit maintenance and solar panel adjustments for around 6-23 days. Both of these reference orbits are perfectly periodic in the CR3BP. For this investigation, the selected reference orbits are then transitioned into the ER3BP using a stacked revolutions approach. To initially transition solutions, a number of revolutions of the 9:2 NRHO and the large DRO in the CR3BP are computed and discretized into a series of patchpoints and segments. These individual arcs are then initialized and propagated in the ER3BP and corrected for position and velocity continuity using a multiple shooting corrections technique. Although some of the reference orbit characteristics shift in the transition process (namely periodicity and initial perilune values), the orbit geometry persists and accurately reflects the motion initially produced in the CR3BP. The 9:2 NRHO and large DRO CR3BP orbits are plotted in Figures 3(a) and 4(a) and their ER3BP equivalents are plotted in Figures 3(b) and 4(b). In the ER3BP reference orbits, it is observed that the libration points oscillate with time with the varying relative distance between the Earth and the Moon.

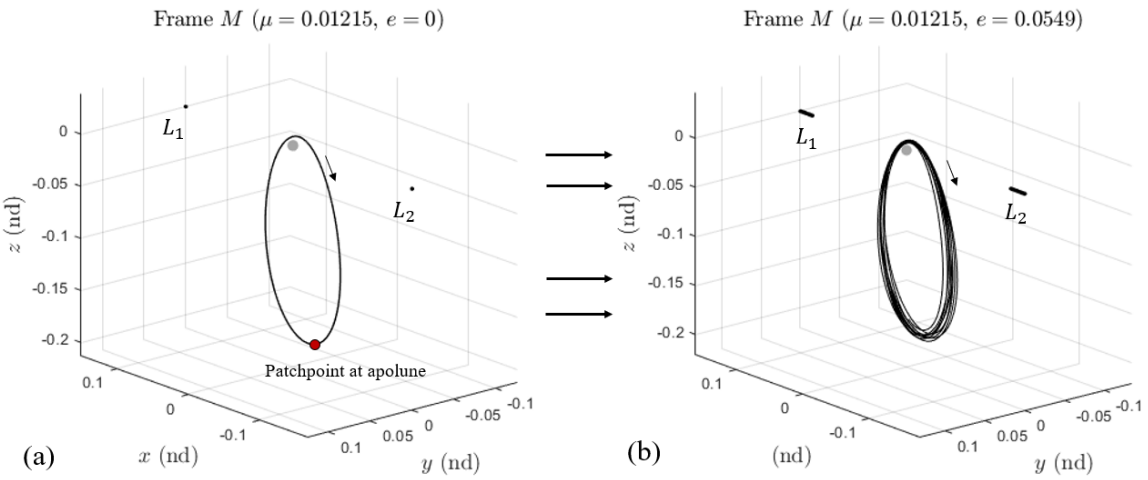

Figure 3. 9:2 NRHO in the CR3BP with the selected patchpoint (left) and its ER3BP equivalent (right) for 9 revolutions.

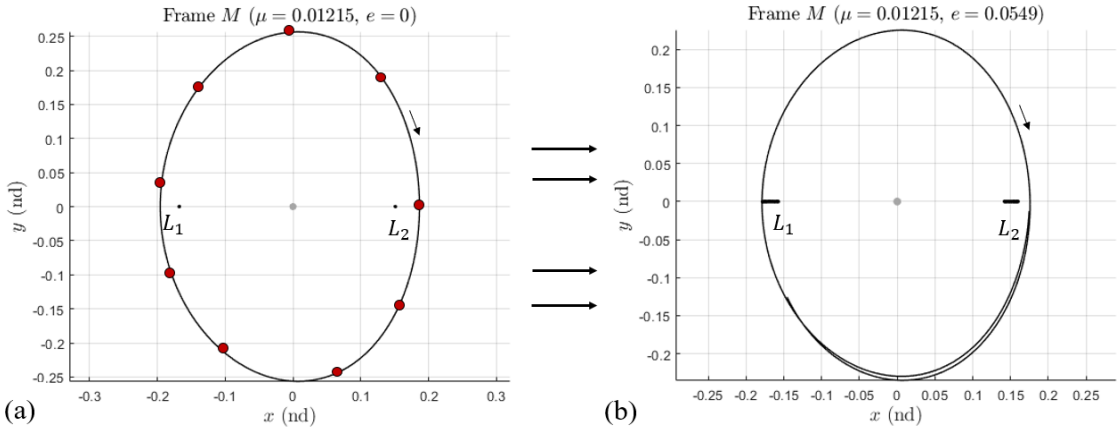

Figure 4. The large DRO in the CR3BP with the selected patchpoints (left) and its ER3BP equivalent (right) for 2 revolutions.

RELATIVE MOTION MODEL

The formulation of the equations of relative motion first necessitates a description of the LVLH frame L. There are a variety of definitions for this local frame. In this investigation, the description in Figure 5 is employed. The LVLH frame is useful for relative motion analysis since it characterizes the relative dynamics of a chaser spacecraft with respect to a target. Consider the following formulation comprised of vectors denoting the target state relative to the central body, i.e.,

$$\hat{\mathbf{i}} = \hat{\mathbf{j}} \times \hat{\mathbf{k}} \qquad \hat{\mathbf{j}} = -\frac{\mathbf{h}}{h} \qquad \hat{\mathbf{k}} = -\frac{\mathbf{r}}{r}$$

In this LVLH framework, $\mathbf{r}$ denotes the target position vector from the central body, $\mathbf{h}$ is the target instantaneous specific angular momentum vector computed as $\mathbf{h} = \mathbf{r} \times \mathbf{v}$, where $\mathbf{v}$ is the target relative velocity vector as measured from the central body. These directions are sometimes labeled as V-BAR ($\hat{\mathbf{i}}$), H-BAR ($\hat{\mathbf{j}}$), and R-BAR ($\hat{\mathbf{k}}$), respectively.

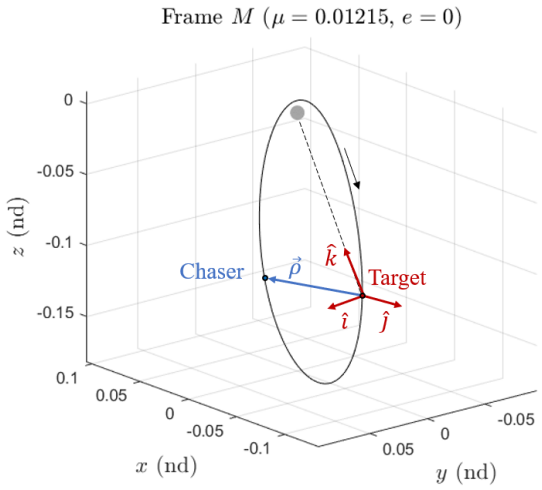

Figure 5. The LVLH frame attached to a target spacecraft with its associated directions

The nonlinear equations of relative motion are formulated to characterize the relative dynamics between a chaser and target subject to the gravitational influence from the Earth and the Moon. The equations governing the motion for both spacecraft with respect to the Moon are expressed as

$$\left[\ddot{\mathbf{r}}\right]_I = -\mu\frac{\mathbf{r}}{r^3} - (1-\mu)\left(\frac{\mathbf{r}+\mathbf{r}_{em}}{||\mathbf{r}+\mathbf{r}_{em}||^3} - \frac{\mathbf{r}_{em}}{r_{em}^3}\right) \tag{35}$$

$$\left[\ddot{\mathbf{r}}_c\right]_I = -\mu\frac{\mathbf{r}_c}{r_c^3} - (1-\mu)\left(\frac{\mathbf{r}_c+\mathbf{r}_{em}}{||\mathbf{r}_c+\mathbf{r}_{em}||^3} - \frac{\mathbf{r}_{em}}{r_{em}^3}\right) \tag{36}$$

where $\mathbf{r}$ and $\mathbf{r}_c$ denote the position vector measured from the Moon to the target and chaser, respectively. Moreover, $\mathbf{r}_{em}$ is the position vector from the Earth to the Moon with r_{em} as its scalar norm. Moreover, any derivatives with surrounding brackets such as

$$\underset{I}{\left[\dot{\mathbf{r}}\right]} \;,\; \underset{M}{\left[\dot{\mathbf{r}}\right]} \;,\; \underset{L}{\left[\dot{\mathbf{r}}\right]}$$

include derivatives as observed in the inertial frame I, the Moon frame M, and the LVLH frame L, respectively. Using the geometry depicted in Figure 5, the chaser's position with respect to the Moon is expressed as

$$\mathbf{r}_c = \mathbf{r} + \boldsymbol{\rho} \tag{37}$$

where $\boldsymbol{\rho}$ denotes the relative position vector from the target to the chaser. The time derivatives of Equation (37) in the inertial frame I follow as

$$\underset{I}{\left[\dot{\mathbf{r}}_c\right]} = \underset{I}{\left[\dot{\mathbf{r}}\right]} + \underset{L}{\left[\dot{\boldsymbol{\rho}}\right]} + \boldsymbol{\omega}_{L/I} \times \boldsymbol{\rho} \tag{38}$$

$$\underset{I}{\left[\ddot{\mathbf{r}}_c\right]} = \underset{I}{\left[\ddot{\mathbf{r}}\right]} + \underset{L}{\left[\ddot{\boldsymbol{\rho}}\right]} + 2\boldsymbol{\omega}_{L/I} \times \underset{L}{\left[\dot{\boldsymbol{\rho}}\right]} + \underset{L}{\left[\dot{\boldsymbol{\omega}}_{L/I}\right]} \times \boldsymbol{\rho} + \boldsymbol{\omega}_{L/I} \times (\boldsymbol{\omega}_{L/I} \times \boldsymbol{\rho}) \tag{39}$$

where $\boldsymbol{\omega}_{L/I}$ denotes the angular velocity of the LVLH frame L with respect to the inertial frame I and $\underset{I}{\left[\dot{\boldsymbol{\omega}}_{L/I}\right]} = \underset{L}{\left[\dot{\boldsymbol{\omega}}_{L/I}\right]}$. Substituting Equations (35) and (36) into Equation (39) yields

$$\begin{aligned}\underset{L}{[\ddot{\boldsymbol{\rho}}]} = &-2\boldsymbol{\omega}_{L/I} \times \underset{L}{[\dot{\boldsymbol{\rho}}]} - \underset{L}{[\dot{\boldsymbol{\omega}}_{L/I}]} \times \boldsymbol{\rho} - \boldsymbol{\omega}_{L/I} \times (\boldsymbol{\omega}_{L/I} \times \rho) \\ &+ \mu\left(\frac{\mathbf{r}}{r^3} - \frac{\mathbf{r}+\boldsymbol{\rho}}{||\mathbf{r}+\boldsymbol{\rho}||^3}\right) + (1-\mu)\left(\frac{\mathbf{r}+\mathbf{r}_{em}}{||\mathbf{r}+\mathbf{r}_{em}||^3} - \frac{\mathbf{r}+\boldsymbol{\rho}+\mathbf{r}_{em}}{||\mathbf{r}+\boldsymbol{\rho}+\mathbf{r}_{em}||^3}\right)\end{aligned} \tag{40}$$

denoted as the nonlinear equations of relative motion for the restricted three-body problem (3B-NLERM). The angular velocity and acceleration of the LVLH frame L with respect to the inertial frame I are expressed as

$$\boldsymbol{\omega}_{L/I} = \boldsymbol{\omega}_{L/M} + \boldsymbol{\omega}_{M/I} \tag{41}$$

$$\underset{L}{[\dot{\boldsymbol{\omega}}_{L/I}]} = \underset{L}{[\dot{\boldsymbol{\omega}}_{L/M}]} + \underset{L}{[\dot{\boldsymbol{\omega}}_{M/I}]} = \underset{L}{[\dot{\boldsymbol{\omega}}_{L/M}]} + \underset{M}{[\dot{\boldsymbol{\omega}}_{M/I}]} - \boldsymbol{\omega}_{L/M} \times \boldsymbol{\omega}_{M/I} \tag{42}$$

where $\boldsymbol{\omega}_{L/M}$ and $\boldsymbol{\omega}_{M/I}$ denote the angular velocity and acceleration vector of frame L with respect to frame M and of frame M with respect to frame I, respectively. Equations (40)-(42) constitute a set of time-varying nonlinear equations where

- The target motion around the Moon is characterized by $\mathbf{r}$, $\boldsymbol{\omega}_{L/M}$, and $\underset{L}{[\dot{\boldsymbol{\omega}}_{L/M}]}$
- The Moon orbital motion is described by $\mathbf{r}_{em}$, $\boldsymbol{\omega}_{M/I}$, and $\underset{L}{[\dot{\boldsymbol{\omega}}_{M/I}]}$

Similar to the process outlined in Franzini et al. [1], analytical descriptions of frame L with respect to frame I are produced to describe the components of $\boldsymbol{\omega}_{L/M}$ and $[\underset{L}{\dot{\boldsymbol{\omega}}_{L/M}}]$. The terms in expressions for $\boldsymbol{\omega}_{M/I}$, and $[\underset{L}{\dot{\boldsymbol{\omega}}_{M/I}}]$ are evaluated by employing either the CR3BP or the ER3BP. More details regarding the derivation of the nonlinear equations of relative motion are available in Franzini et al. [1] and Khoury [2]. The angular velocity of frame L with respect to M is expressed as

$$\boldsymbol{\omega}_{L/M} = \omega^y_{L/M}\hat{\mathbf{j}} + \omega^z_{L/M}\hat{\mathbf{k}} \tag{43}$$

$$= \left(-\frac{1}{r}[\underset{M}{\dot{\mathbf{r}}}] \cdot \hat{\mathbf{i}} \right)\hat{\mathbf{j}} + \left(\frac{r}{h}[\underset{M}{\ddot{\mathbf{r}}}] \cdot \hat{\mathbf{j}} \right)\hat{\mathbf{k}} \tag{44}$$

$$= \left(-\frac{h}{r^2} \right)\hat{\mathbf{j}} + \left(-\frac{r}{h^2}\mathbf{h} \cdot [\underset{M}{\ddot{\mathbf{r}}}] \right)\hat{\mathbf{k}} \tag{45}$$

where $[\underset{M}{\ddot{\mathbf{r}}}]$ denotes the target acceleration in frame M expressed as

$$[\underset{M}{\ddot{\mathbf{r}}}] = -2\boldsymbol{\omega}_{M/I} \times [\underset{M}{\dot{\mathbf{r}}}] - [\underset{M}{\dot{\boldsymbol{\omega}}_{M/I}}] \times \mathbf{r} - \boldsymbol{\omega}_{M/I} \times (\boldsymbol{\omega}_{M/I} \times \mathbf{r}) - \mu\frac{\mathbf{r}}{r^3} - (1-\mu)\left(\frac{\mathbf{r} + \mathbf{r}_{em}}{||\mathbf{r} + \mathbf{r}_{em}||^3} - \frac{\mathbf{r}_{em}}{r^3_{em}} \right) \tag{46}$$

The angular acceleration components along the LVLH frame are computed by differentiating the components in Equation (45). Therefore the angular acceleration components are expressed as

$$\dot{\omega}^y_{L/M} = -\frac{1}{r}\left(\frac{\dot{h}}{r} + 2\dot{r}\omega^y_{L/M} \right) \tag{47}$$

$$\dot{\omega}^z_{L/M} = \left(\frac{\dot{r}}{r} - 2\frac{\dot{h}}{h} \right)\omega^z_{L/M} - \frac{r}{h^2}\mathbf{h} \cdot [\underset{M}{\dddot{\mathbf{r}}}] \tag{48}$$

where the following relationships are employed.

$$\dot{r} = \frac{1}{r}\mathbf{r} \cdot [\underset{M}{\dot{\mathbf{r}}}] \qquad \dot{h} = -[\underset{M}{\dot{\mathbf{h}}}] \cdot \hat{\mathbf{j}}$$

and the target jerk is evaluated as

$$\begin{aligned}[\underset{M}{\dddot{\mathbf{r}}}] = {} & -2\boldsymbol{\omega}_{M/I} \times [\underset{M}{\ddot{\mathbf{r}}}] - 3[\underset{M}{\dot{\boldsymbol{\omega}}_{M/I}}] \times [\underset{M}{\dot{\mathbf{r}}}] - [\underset{M}{\ddot{\boldsymbol{\omega}}_{M/I}}] \times \mathbf{r} - [\underset{M}{\dot{\boldsymbol{\omega}}_{M/I}}] \times (\boldsymbol{\omega}_{M/I} \times \mathbf{r}) - \boldsymbol{\omega}_{M/I} \times ([\underset{M}{\dot{\boldsymbol{\omega}}_{M/I}}] \times \mathbf{r}) \\ & - \boldsymbol{\omega}_{M/I} \times (\boldsymbol{\omega}_{M/I} \times [\underset{M}{\dot{\mathbf{r}}}]) - \mu\frac{\partial}{\partial \mathbf{r}}\left[\frac{\mathbf{r}}{r^3} \right][\underset{M}{\dot{\mathbf{r}}}] - (1-\mu)\frac{\partial}{\partial \mathbf{r}}\left[\frac{\mathbf{r} + \mathbf{r}_{em}}{||\mathbf{r} + \mathbf{r}_{em}||^3} \right]([\underset{M}{\dot{\mathbf{r}}}] + [\underset{M}{\dot{\mathbf{r}}_{em}}]) \\ & + (1-\mu)\frac{\partial}{\partial \mathbf{r}_{em}}\left[\frac{\mathbf{r}_{em}}{r^3_{em}} \right][\underset{M}{\dot{\mathbf{r}}_{em}}]\end{aligned} \tag{49}$$

where

$$\underset{M}{[\dot{\mathbf{r}}_{em}]} = \underset{I}{[\dot{\mathbf{r}}_{em}]} - \boldsymbol{\omega}_{M/I} \times \mathbf{r}_{em}$$

and

$$\frac{\partial}{\partial \mathbf{q}}\left[\frac{\mathbf{q}}{q^3}\right] = \frac{1}{q^3}\left(\mathbf{I} - 3\frac{\mathbf{q}\mathbf{q}^T}{q^2}\right)$$

In conclusion, the angular components of the LVLH frame angular velocity and accelerations are expressed in terms of kinematic relationships between the two frames with quantities computed in frame M.

CR3BP Assumption

Simplifications to the 3B-NLERM are incorporated by assuming that the two primaries, namely the Earth and the Moon, are described using the CR3BP. As a result, a number of the time-varying parameters are reduced to zero, such that

- The position vector from the Earth to the Moon is $\mathbf{r}_{em} = -\hat{\mathbf{i}}_m$
- The velocity vector from the Earth to the Moon is $\underset{M}{[\dot{\mathbf{r}}_{em}]} = \mathbf{0}$
- The angular velocity of frame M with respect to frame I is $\boldsymbol{\omega}_{M/I} = \hat{\mathbf{k}}_m$
- The angular acceleration of frame M with respect to frame I is $\underset{M}{[\dot{\boldsymbol{\omega}}_{M/I}]} = \mathbf{0}$
- The derivative of the angular acceleration of frame M with respect to frame I is $\underset{M}{[\ddot{\boldsymbol{\omega}}_{M/I}]} = \mathbf{0}$

where the quantities $\mathbf{r}_{em}$ and $\boldsymbol{\omega}_{M/I}$ possess unitary norms due to the employment of the nondimensional quantities. The equations of relative motion in frame L are, thus, obtained by evaluating the angular velocity and acceleration components using the formulated analytical expressions. To implement the equations, the following state vector is defined such that

$$\mathbf{X}_{\text{state}} = \Big[f_{\text{M}},\ r_{x,M},\ r_{y,M},\ r_{z,M},\ v_{x,M},\ v_{y,M},\ v_{z,M},\ \ x,\ y,\ z,\ \dot{x},\ \dot{y},\ \dot{z},\ \omega_y,\ \omega_z \Big]^T$$

where f_M is the Moon's true anomaly, $r_{i,M}$ denotes the target position in Frame M, $v_{i,M}$ denotes the target velocity in Frame M, x, y, z define the elements of the relative position vector, $\dot{x}, \dot{y}, \dot{z}$ are components of the relative velocity vector, and ω_y, ω_z are the angular velocity components of frame L with respect to frame M.

Linearized Equations of Relative Motion

As proposed in Franzini et al. [1], the nonlinear relative equations of motion, 3B-NLERM, are further simplified by linearizing the gravitational accelerations around the target position. To summarize the relative motion sets, two skew symmetric matrices that contain components of the angular velocity and acceleration vectors are introduced such that

$$\mathbf{\Omega}_{L/I} = \begin{bmatrix} 0 & -\omega^z_{L/I} & \omega^y_{L/I} \\ \omega^z_{L/I} & 0 & -\omega^x_{L/I} \\ -\omega^y_{L/I} & \omega^x_{L/I} & 0 \end{bmatrix} \qquad \dot{\mathbf{\Omega}}_{L/I} = \begin{bmatrix} 0 & -\dot{\omega}^z_{L/I} & \dot{\omega}^y_{L/I} \\ \dot{\omega}^z_{L/I} & 0 & -\dot{\omega}^x_{L/I} \\ -\dot{\omega}^y_{L/I} & \dot{\omega}^x_{L/I} & 0 \end{bmatrix}$$

where

$$\boldsymbol{\omega}_{L/I} = \omega^x_{L/I}\hat{\mathbf{i}} + \omega^y_{L/I}\hat{\mathbf{j}} + \omega^z_{L/I}\hat{\mathbf{k}} \qquad \underset{L}{[\dot{\boldsymbol{\omega}}_{L/I}]} = \dot{\omega}^x_{L/I}\hat{\mathbf{i}} + \dot{\omega}^y_{L/I}\hat{\mathbf{j}} + \dot{\omega}^z_{L/I}\hat{\mathbf{k}}$$

The skew symmetric matrices allow the relative motion sets to be written more compactly. The distinction between the relative motion sets used in the ER3BP and CR3BP is accomplished by the assumptions characterizing the Earth-Moon motion. As a result, the three-body elliptical nonlinear equations of motion or 3B-ENLERM are implemented to describe the relative dynamics as

$$\underset{L}{[\ddot{\boldsymbol{\rho}}]} = -2\mathbf{\Omega}_{L/I}\underset{L}{[\dot{\boldsymbol{\rho}}]} - (\underset{L}{[\dot{\mathbf{\Omega}}_{L/I}]} + \mathbf{\Omega}^2_{L/I})\boldsymbol{\rho} + \mu\left(\frac{\mathbf{r}}{r^3} - \frac{\mathbf{r}+\boldsymbol{\rho}}{||\mathbf{r}+\boldsymbol{\rho}||^3}\right) + (1-\mu)\left(\frac{\mathbf{r}+\mathbf{r}_{em}}{||\mathbf{r}+\mathbf{r}_{em}||^3} - \frac{\mathbf{r}+\boldsymbol{\rho}+\mathbf{r}_{em}}{||\mathbf{r}+\boldsymbol{\rho}+\mathbf{r}_{em}||^3}\right) \tag{50}$$

The equations of motion are further expressed as a nonlinear system, assuming that the chaser is maneuverable by a control vector $\mathbf{u}(\tau)$. Thus, Equation (50) is written

$$\dot{\mathbf{x}}(\tau) = \mathbf{f}(\tau, \mathbf{x}(\tau)) + \mathbf{B}\mathbf{u}(\tau) \tag{51}$$

where

$$\mathbf{x}(\tau) = \begin{bmatrix} \boldsymbol{\rho}(\tau) \\ \underset{L}{[\dot{\boldsymbol{\rho}}(\tau)]} \end{bmatrix} \quad \text{and} \quad \mathbf{B} = \begin{bmatrix} \mathbf{0}_{3\times3} \\ \mathbf{I}_{3\times3} \end{bmatrix}$$

and $\mathbf{x}(\tau) \in \mathbb{R}^6$, $\mathbf{f} : [0, +\infty) \times \mathbb{R}^6 \to \mathbb{R}^6$, $\mathbf{B} \in \mathbb{R}^{6\times3}$. Moreover, the gravitational acceleration terms linearized around the target position are used to obtain the three body linear relative equations of motion or 3B-LERM as

$$\underset{L}{[\ddot{\boldsymbol{\rho}}]} = -2\boldsymbol{\Omega}_{L/I}\underset{L}{[\dot{\boldsymbol{\rho}}]} - \left(\underset{L}{[\dot{\boldsymbol{\Omega}}_{L/I}]} + \boldsymbol{\Omega}_{L/I}^2 + \frac{\mu}{r^3}\left(\mathbf{I} - 3\frac{\mathbf{r}\mathbf{r}^T}{r^2}\right) + \frac{1-\mu}{||\mathbf{r}+\mathbf{r}_{em}||^3}\left(\mathbf{I} - 3\frac{(\mathbf{r}+\mathbf{r}_{em})(\mathbf{r}+\mathbf{r}_{em})^T}{||\mathbf{r}+\mathbf{r}_{em}||^2}\right)\right)\boldsymbol{\rho} \tag{52}$$

Additionally, Equation (52) is written in state-space form such that

$$\dot{\mathbf{x}}(\tau) = \mathbf{A}(\tau)\mathbf{x}(\tau) + \mathbf{B}\mathbf{u}(\tau) \tag{53}$$

where the system matrix $\mathbf{A}(\tau)$ is defined as

$$\mathbf{A}(\tau) = \begin{bmatrix} \mathbf{0}_{3\times3} & \mathbf{I}_{3\times3} \\ \mathbf{A}_{\boldsymbol{\rho}\dot{\boldsymbol{\rho}}}(\tau) & -2\boldsymbol{\Omega}_{L/I}(\tau) \end{bmatrix}$$

and

$$\begin{aligned}\mathbf{A}_{\boldsymbol{\rho}\dot{\boldsymbol{\rho}}}(\tau) = &-\underset{L}{[\dot{\boldsymbol{\Omega}}_{L/I}(\tau)]} - \boldsymbol{\Omega}_{L/I}(\tau)^2 - \frac{\mu}{r(\tau)^3}\left(\mathbf{I} - 3\frac{\mathbf{r}(\tau)\mathbf{r}(\tau)^T}{r(\tau)^2}\right) \\ &+ \frac{1-\mu}{||\mathbf{r}(\tau)+\mathbf{r}_{em}(\tau)||^3}\left(\mathbf{I} - 3\frac{(\mathbf{r}(\tau)+\mathbf{r}_{em}(\tau))(\mathbf{r}(\tau)+\mathbf{r}_{em}(\tau))^T}{||\mathbf{r}(\tau)+\mathbf{r}_{em}(\tau)||^2}\right)\end{aligned}$$

The system matrix is available to construct the relative state transition matrix (RSTM) to implement a shooting scheme for targeting relative states with respect to the target spacecraft. The advantage of targeting states in the LVLH frame L originates from the ability to deliver desired relative motion from the perspective of the target.

APPLICATION: ORBITAL RENDEZVOUS

A number of rendezvous examples are examined in this investigation. In each rendezvous example, two plots are provided. In each figure, plot (a) indicates the target starting mean anomaly along the reference orbit. The blue and red circles denote the starting positions of the chaser and target, respectively. The red star identifies the final position of the target. The red line depicts the path of the target along the reference orbit and the blue line is the rendezvous trajectory by the chaser to intercept the target. Plot (b) illustrates the relative dynamics in the LVLH frame L. The origin of the LVLH frame is defined as the target and is indicated by the red star. The arrows depict the direction of motion. In each of the reference orbits, the eccentricity of the system is included in the plots to denote the model employed in the simulation. Previous analyses of the relative equations of motion indicate that the 3B-LERM simulations are most accurate near regions of apolune. Figures 7 - 8 reflect the sample rendezvous in the ER3BP for the 9:2 NRHO as the baseline. Likewise, rendezvous scenarios are plotted for the ER3BP Large DRO as the baseline in Figures 9- 10. A comparison of the solutions in both the CR3BP and ER3BP reference orbits is provided in Table 2. A two impulsive maneuver scheme, the first to initialize the rendezvous maneuver and the second to eliminate any excess velocity at the interception point is assumed in this investigation.

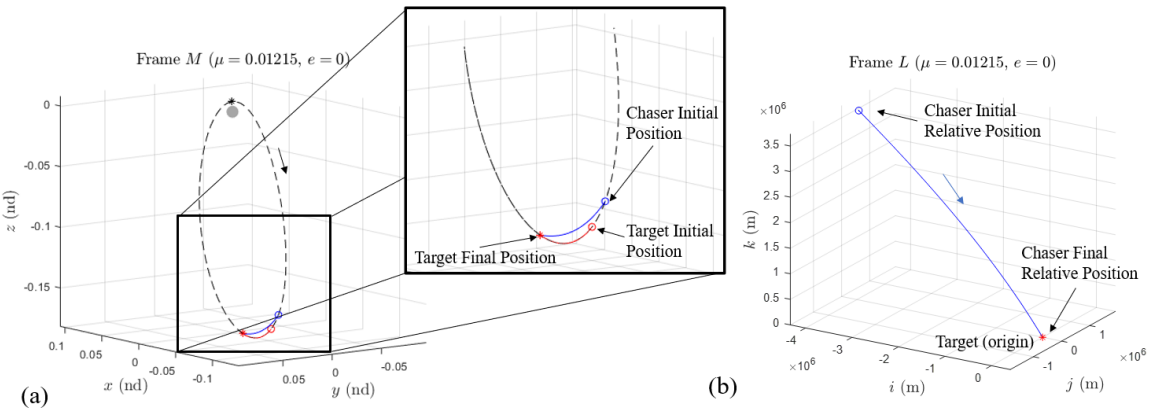

Figure 6. 9:2 NRHO Rendezvous Schematic

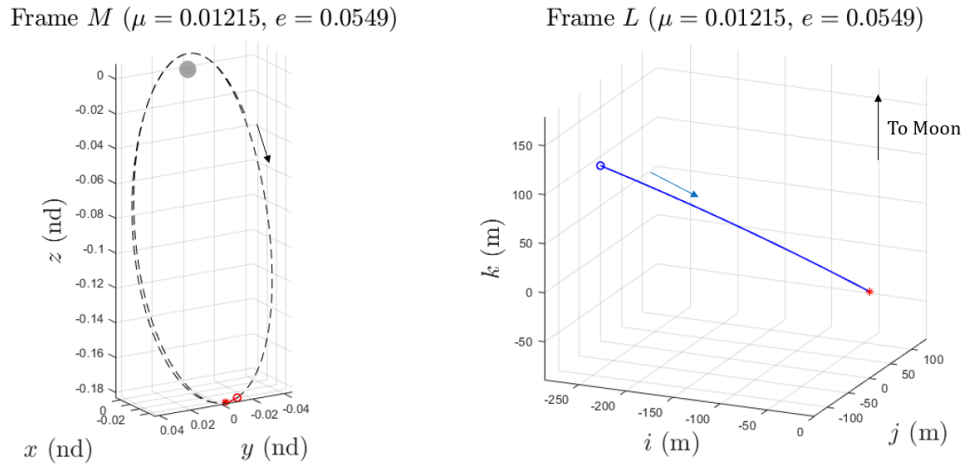

Figure 7. 9:2 NRHO: target $MA = 162°$, 300 m (behind target)

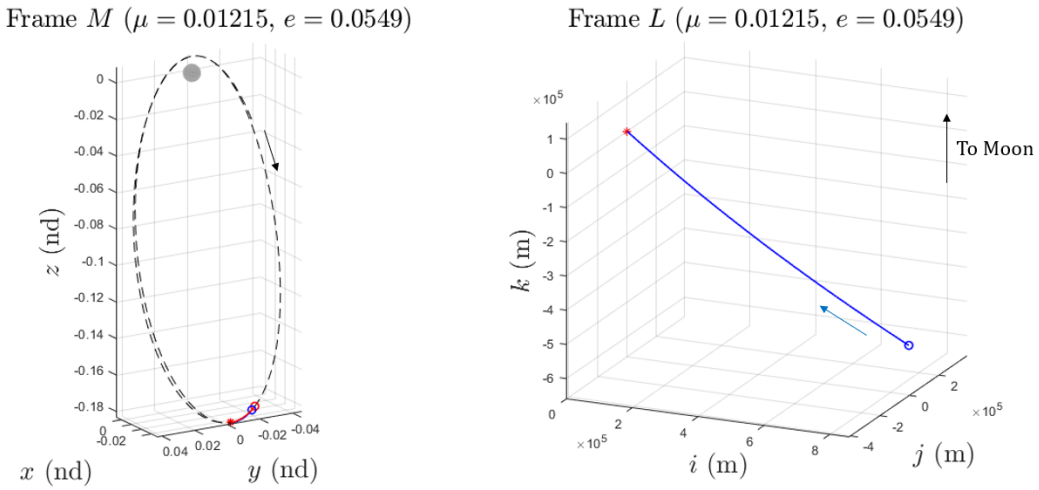

Figure 8. 9:2 NRHO: target $MA = 144°$, 1000 km (ahead target)

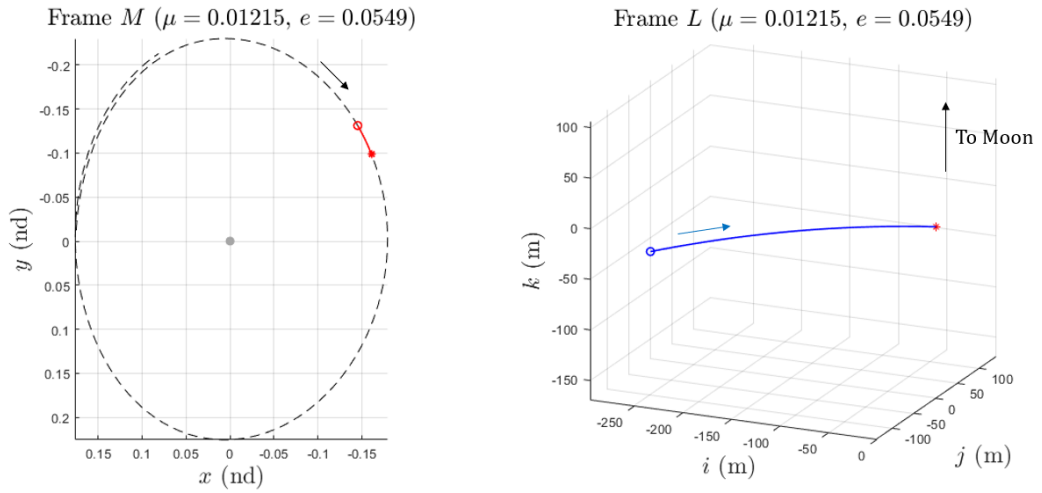

Figure 9. Large DRO: target $MA = 90°$, 300 m (behind target)

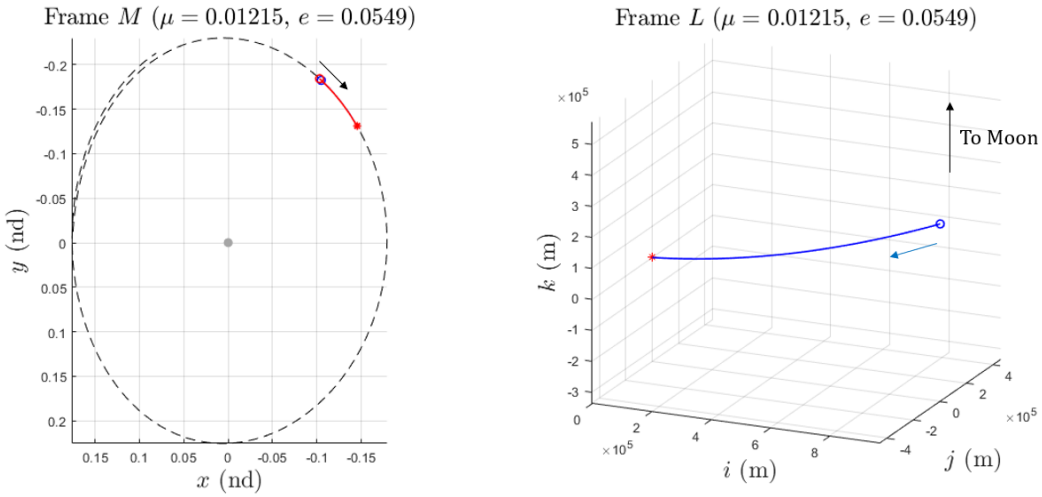

Figure 10. Large DRO: target $MA = 72°$, 1000 km (ahead target)

Table 1. Rendezvous Maneuver Results

Reference Orbit	**Model**	Δv_1 [m/s]	Δv_2 [m/s]	Δv_{tot} [m/s]
9:2 NRHO, Figures 7 300 m - Behind, TOF: 8 hrs.	CR3BP	0.01	0.01	0.02
	ER3BP	0.01	0.01	0.02
9:2 NRHO, Figures 8 1000 km - Ahead, TOF: 16 hrs.	CR3BP	14.769	17.429	32.198
	ER3BP	14.885	17.432	32.316

Table 2. Rendezvous Maneuver Results

Reference Orbit	**Model**	Δv_1 [m/s]	Δv_2 [m/s]	Δv_{tot} [m/s]
Large DRO, Figures 9 300 m - Behind, TOF: 8 hrs.	CR3BP	0.011	0.011	0.021
	ER3BP	0.011	0.011	0.021
Large DRO, Figures 10 1000 km - Ahead, TOF: 16 hrs.	CR3BP	19.146	17.404	36.550
	ER3BP	18.959	17.455	36.415

From the results for the rendezvous scenarios in both the 9:2 NRHO and large DRO, it is observed that the differences between the CR3BP and ER3BP are more evident in scenarios involving a larger initial distance between the target and chaser. The slight differences in the reference geometries between the CR3BP and ER3BP are more apparent on scales involving larger distances, yet the magnitude of the Δv maneuvers only vary on the order of centimeters per second in the relative velocity. The sample scenarios in Figures 7 - 10 demonstrate that terminal rendezvous is achieved in configurations where the chaser moves as close as 300 meters to as far as 1000 km in initial relative distance from the target. Moreover, scenarios involving the chaser both behind and ahead of the target are also successful.

APPLICATION: SPACECRAFT LOITERING

Another application for the relative motion in this investigation is spacecraft loitering. The typical aim for loitering is producing bounded relative motion of the chaser in the LVLH Frame L with respect to the target spacecraft. Such behaviors is accomplished through natural loitering where the motion of the chaser trajectory is bounded in frame L without the implementation of maneuvers. The principle behind natural loitering is based on an approach such that the target and chaser are placed along the same reference trajectory but at different mean anomalies; their relative motion then remains bounded. In this investigation, spacecraft loitering is examined for vehicles in the 9:2 NRHO and large DRO in the CR3BP and ER3BP. As an example, consider the target and chaser along a 9:2 NRHO in the CR3BP but at different initial mean anomalies. The initial positions of the target and chaser are plotted in Figure 11(a) and denoted with the red and blue circles, respectively. The starred points represent the target and chaser position after one full period of the NRHO, thus, they arrive at the initial point at the final time. Likewise, in Figure 11(b), the relative motion with the blue circle denotes the initial chaser position.

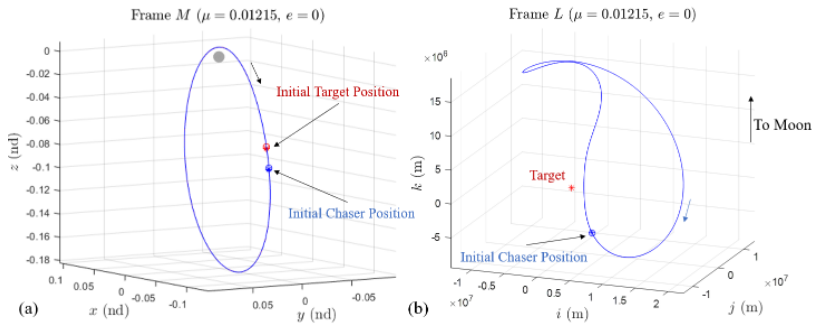

Figure 11. 9:2 NRHO Loitering Description

Spacecraft loitering is also accomplished involving the execution of multiple maneuvers to produce bounded relative motion in the LVLH frame L. In contrast to natural loitering, forced loitering allows for more variation in the relative geometry since the chaser implements maneuvers in the vicinity of the target. The forced loitering approach employs a multiple shooting corrections scheme where state variables are expressed in terms of the local frame. A relative trajectory is discretized into a number of trajectory segments and patchpoints. The patchpoints are selected positions in relative space with respect to the target and can be specified at some relative distance along the LVLH axes. The "relative" multiple shooter is employed to correct with a goal for relative position continuity, yet it allows the relative velocity at patchpoints to vary indicating the presence of a maneuver. In this investigation, forced loitering approaches are examined for the 9:2 NRHO and large DRO in both the CR3BP and the ER3BP. In each sample scenario, plot (a) in Frame M indicates the starting location of the target along the corresponding reference orbit. The chaser is placed at an initial relative distance from the target and both are propagated for a set time of flight. Correspondingly, plot (b) appears as viewed in Frame L to depict the relative motion between the spacecraft over the propagation time. The starred locations along the trajectory indicate a maneuver to ensure that the chaser intercepts its next specified patchpoint. As an example, a forced loitering scenario appears in Figure 12 in the 9:2 NRHO for the CR3BP. Initial locations of the chaser and target are specified along with the locations of each maneuver corresponding to the selected relative patchpoints. Certain relative geometries, e.g. the "diamond" shape, are produced as a proof of concept for the forced loitering approach. In practice, any combination of relative patchpoints can be used and forced loitering is then useful prior to a close approach between the two spacecraft; thus, the chaser may 'orbit' the target for some initial duration before proceeding to pther phases, perhaps terminal rendezvous. Moreover, a forced loitering approach ensures collision avoidance by specifying a loitering geometry at a minimum relative distance between the spacecraft. In either natural or forced loitering, relative geometries are depicted from the perspective of the target, useful for establishing a baseline intuition regarding the relative behavior of the spacecraft along the different reference orbits in more complex dynamical regimes.

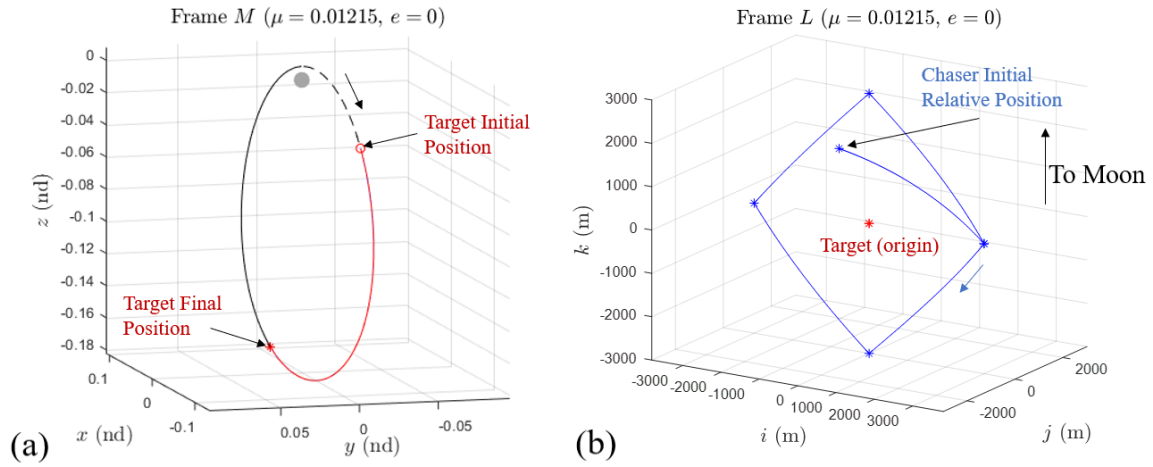

Figure 12. Forced loitering example in the 9:2 NRHO

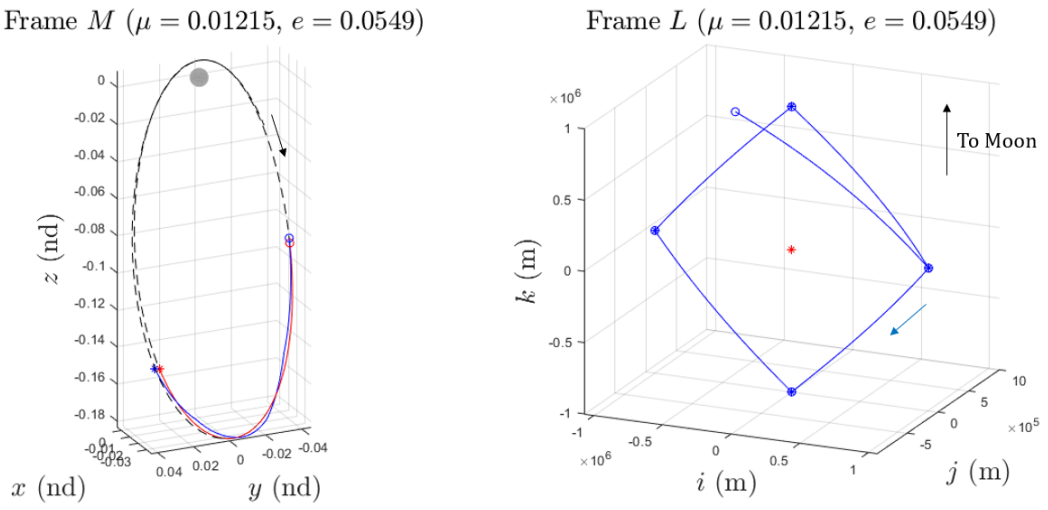

Figure 13. 9:2 NRHO Loiter at 1000 km in ER3BP

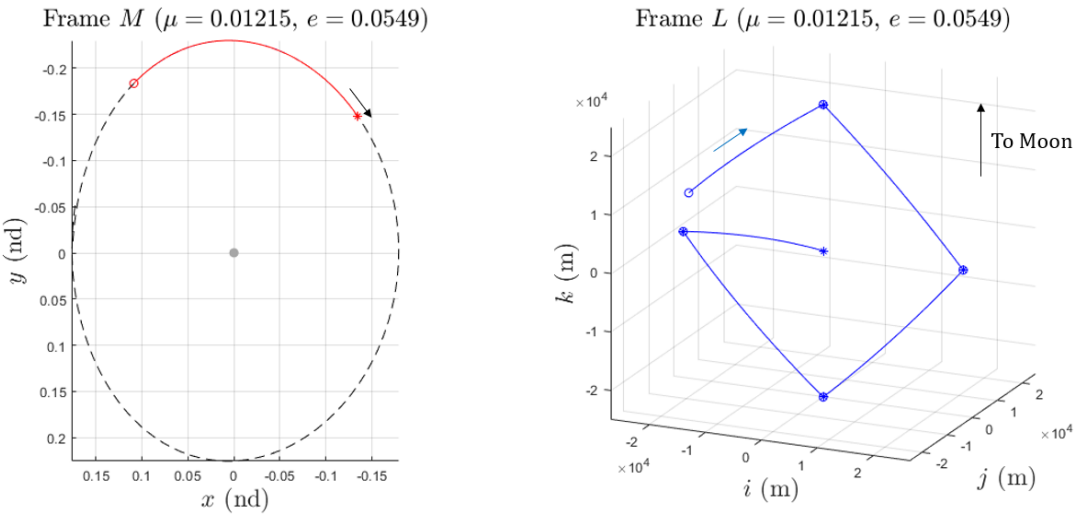

Figure 14. Large DRO Loiter at 10 km in ER3BP

Table 3. Forced Loitering Case Descriptions with Δv magnitudes

Reference Orbit	Model	Δv_1 [m/s]	Δv_2 [m/s]	Δv_3 [m/s]	Δv_4 [m/s]	Δv_5 [m/s]	Δv_{tot} [m/s]
9:2 NRHO , 1000 km Loiter Figure 13 , TOF (total): 100 hrs.	CR3BP	20.093	28.715	27.098	24.766	27.136	127.808
	ER3BP	20.242	28.848	27.019	24.726	27.000	127.836
Large DRO , 25 km Loiter Figure 14 , TOF (total): 75 hrs.	CR3BP	0.534	0.718	0.884	0.877	1.012	4.026
	ER3BP	0.569	0.731	0.863	0.852	0.990	4.004

The results presented in Table 3 summarize the approximate Δvs that are required to produce

the desired relative geometries for the sample scenarios in each of the reference orbits. There is no significant difference between approximations in the CR3BP and ER3BP and they produce nearly identical loitering geometry. The benefit of forced loitering includes more variation in the loitering geometry through the implementation of multiple chaser maneuvers about the target. Although requiring higher propellant use, relative distances between the target and chaser are maintained for an extended time interval.

CONCLUDING REMARKS

In this investigation, a number of rendezvous and spacecraft loitering problems are examined for the Earth-Moon system. First, a description of the Earth-Moon system using the CR3BP and ER3BP are introduced. Reference solutions are produced in both dynamical regimes employing the 9:2 L_2 NRHO and a large DRO as the baseline orbits for NASA' s proposed Artemis missions. The equations of relative motion are formulated in a LVLH frame attached to a target spacecraft. The linear variational counterpart for the equations of relative motion is used to construct targeting schemes in the LVLH frame. Rendezvous scenarios for the 9:2 NRHO and large DRO are investigated and comparisons between the results in the CR3BP and ER3BP. Finally, natural and forced spacecraft loitering is also examined to produce bounded and predictable relative motion with respect to the target. A transition of the solutions obtained in the CR3BP and ER3BP into a higher-fidelity ephemeris model is a next step.

REFERENCES

[1] G. Franzini and M. Innocenti, "Relative motion equations in the localvertical local-horizon frame for rendezvous in lunar orbits", in Proc. 2017 AAS/AIAA Astrodynamics Specialist Conference, Stevenson,WA, USA, Aug. 2017, Paper AAS 17-641.

[2] Khoury, Fouad. MSAAE, Purdue University, August 2020. Orbital Rendezvous and Spacecraft Loitering in the Earth-Moon system.

[3] W. H. Clohessy and R. S. Wiltshire, "Terminal guidance system for satellite rendezvous," Journal of the Aerospace Sciences, vol. 27, no. 9, pp. 653–658, 1960.

[4] K. Yamanaka and F. Ankersen, "New state transition matrix for relative motion on an arbitrary elliptical orbit," Journal of Guidance, Control, and Dynamics, vol. 25, no. 1, pp. 60–66, 2002.

[5] Franzini, Giovanni. PhD Thesis, Universita di Pisa, May 2018. Relative Motion Dynamics and Control in the Two-Body and in the Restricted Three-Body Problem.

[6] W. S. Koon, M. W. Lo, J. E. Marsden, and S. D. Ross, Dynamical Systems, the Three-Body Problem and Space Mission Design. Marsden Books, 2011.

[7] E. M. Zimovan, K. C. Howell, and D. C. Davis, "Near rectilinear halo orbits and their application in cis-lunar space," in Proc. 3rd IAA Conference on Dynamics and Control of Space Systems, Moscow, Russia, May 2017, Paper IAA-AAS-DyCoSS3-125.

[8] D. Guzzetti, E. M. Zimovan, K. C. Howell, and D. C. Davis, "Stationkeeping analysis for spacecraft in lunar near rectilinear halo orbits," in Advances in the Astronautical Sciences, vol. 160, 2017, pp. 3199–3218, Paper AAS 17-395.

[9] A. Colagrossi, M. Lavagna, and S. F. R. Carna, "Dynamical analysis of rendezvous and docking with very large space infrastructures in non-Keplerian orbits," in Proc. 6th International Conference on Astrodynamics Tools and Techniques, Darmstadt, Germany, Mar. 2016.

[10] K. T. Alfriend, S. R. Vadali, P. Gurfil, J. P. How, and L. S. Breger, Spacecraft Formation Flying. Elsevier, 2010.

[11] J. Sullivan, S. Grimberg, and S. D'Amico, "Comprehensive survey and assessment of spacecraft relative motion dynamics models," Journal of Guidance, Control, and Dynamics, vol. 40, no. 8, pp. 1837–1859, 2017.

[12] W. Fehse, Automated Rendezvous and Docking of Spacecraft. New York: Cambridge University Press, 2003.

[13] Victor Szebehely. Theory of Orbits: The Restricted Problem of Three Bodies. Academic Press, Inc., New York, 1967.